Atmospheric Environment 203 (2019) 196–205

Contents lists available at ScienceDirect

Atmospheric Environment

journal homepage: www.elsevier.com/locate/atmosenv

Impacts of local vs. trans-boundary emissions from different sectors on $PM_{2.5}$ exposure in South Korea during the KORUS-AQ campaign

Jinkyul Choi[a], Rokjin J. Park[a,*], Hyung-Min Lee[a], Seungun Lee[a], Duseong S. Jo[b,c], Jaein I. Jeong[a], Daven K. Henze[d], Jung-Hun Woo[e], Soo-Jin Ban[f], Min-Do Lee[f], Cheol-Soo Lim[f], Mi-Kyung Park[f], Hye J. Shin[f], Seogju Cho[g], David Peterson[h], Chang-Keun Song[i,**]

[a] School of Earth and Environmental Sciences, Seoul National University, Seoul, Republic of Korea
[b] Cooperative Institute for Research in Environmental Sciences, University of Colorado, Boulder, CO, USA
[c] Department of Chemistry & Biochemistry, University of Colorado, Boulder, CO, USA
[d] Department of Mechanical Engineering, University of Colorado, Boulder, CO, USA
[e] Department of New Technology and Fusion (DATF), Konkuk University, Seoul, Republic of Korea
[f] National Institute of Environmental Research (NIER), Incheon, Republic of Korea
[g] Seoul Metropolitan Government Research Institute of Public Health and Environment (SIHE), Gyeonggi-do, Republic of Korea
[h] U.S. Naval Research Laboratory, Monterey, CA, USA
[i] Ulsan National Institute of Science and Technology (UNIST), Ulsan, Republic of Korea

ARTICLE INFO

Keywords:
Trans-boundary emissions
$PM_{2.5}$ exposure
Source attribution
KORUS-AQ

ABSTRACT

High concentrations of $PM_{2.5}$ have become a serious environmental issue in South Korea, which ranked 1st or 2nd among OECD countries in terms of population exposure to $PM_{2.5}$. Quantitative understanding of $PM_{2.5}$ source attribution is thus crucial for developing efficient air quality mitigation strategies. Here we use a suite of extensive observations of $PM_{2.5}$ and its precursors concentrations during the international KORea-US cooperative Air Quality field study in Korea (KORUS-AQ) in May–June 2016 to investigate source contributions to $PM_{2.5}$ in South Korea under various meteorological conditions. For the quantitative analysis, we updated a 3-D chemical transport model, GEOS-Chem, and its adjoint with the latest regional emission inventory and other recent findings. The updated model is evaluated by comparing against observed daily $PM_{2.5}$ and its component concentrations from six ground sites (Bangnyung, Bulkwang, Olympic park, Gwangju, Ulsan, and Jeju). Overall, simulated concentrations of daily $PM_{2.5}$ and its components are in a good agreement with observations over the peninsula. We conduct an adjoint sensitivity analysis for simulated surface level $PM_{2.5}$ concentrations at five ground sites (except for Bangnyung because of its small population) under four different meteorological conditions: dynamic weather, stagnant, extreme pollution, and blocking periods. Source contributions by regions vary greatly depending on synoptic meteorological conditions. Chinese contribution accounts for almost 68% of $PM_{2.5}$ in surface air in South Korea during the extreme pollution period of the campaign, whereas an enhanced contribution from domestic sources (57%) occurs for the blocking period. Results from our sensitivity analysis suggest that the reduction of domestic anthropogenic NH_3 emissions could be most effective in reducing population exposure to $PM_{2.5}$ in South Korea (effectiveness = 14%) followed by anthropogenic SO_2 emissions from Shandong region (effectiveness = 11%), domestic anthropogenic NO_x emissions (effectiveness = 10%), anthropogenic NH_3 emissions from Shandong region (effectiveness = 8%), anthropogenic NO_x emissions from Shandong region (effectiveness = 7%), domestic anthropogenic OC emissions (effectiveness = 7%), and domestic anthropogenic BC emissions (effectiveness = 5%).

1. Introduction

Airborne fine particulate matter (e.g., $PM_{2.5}$) is detrimental to human health by causing respiratory and cardiovascular diseases (e.g., Pope III et al., 2002; Laden et al., 2006). In particular, long-term exposure to $PM_{2.5}$ increases population mortality (e.g., Pope III et al.,

* Corresponding author.
** Corresponding author.
E-mail addresses: rjpark@snu.ac.kr (R.J. Park), cksong@unist.ac.kr (C.-K. Song).

https://doi.org/10.1016/j.atmosenv.2019.02.008
Received 2 September 2018; Received in revised form 19 December 2018; Accepted 1 February 2019
Available online 11 February 2019
1352-2310/

2002; Miller et al., 2007; Beelen et al., 2008). No safe level for $PM_{2.5}$ has been identified below which human health is not damaged (WHO Regional Office for Europe, 2013).

$PM_{2.5}$ is a mixture of solid and liquid particles suspended in the air with diameter less than 2.5 μm. Major chemical constituents of $PM_{2.5}$ include nitrates (NO_3^-), sulfates (SO_4^{2-}), ammonium (NH_4^+), organic carbon (OC), and black carbon (BC). They can either be directly emitted or chemically produced in the air by the reactions of its precursors such as nitrogen oxides (NO_x), sulfur dioxide (SO_2), and ammonia (NH_3), emitted from both anthropogenic and natural sources. $PM_{2.5}$ has a lifetime of days to weeks and can even be transported for over hundred or thousand kilometers, crossing boundaries of regions, countries, and even continents (Park et al., 2004; Weber et al., 2007; Hodzic et al., 2007).

High concentrations of $PM_{2.5}$ have become a serious environmental issue in South Korea, which ranked 1st or 2nd among OECD countries in terms of population exposure to $PM_{2.5}$ (OECD, 2018; WHO, 2016). In order to improve the PM air quality in South Korea, the government enacted enforcement decree of the framework act on environmental policy in 2018. The act includes environmental standards for $PM_{2.5}$, which should not exceed 15 $\mu g\ m^{-3}$ on an annual mean basis, and 35 $\mu g\ m^{-3}$ for a 24-h average concentration.

Quantitative understanding of source attribution to $PM_{2.5}$ concentrations in South Korea is thus crucial for developing efficient air quality mitigation strategies. South Korea's rapid economic growth in the past is one contributing factor to high $PM_{2.5}$. However, there are also many outside sources such as soil dust from desert areas, anthropogenic pollution from upwind China, and biomass burning from Siberia. Along with dynamic synoptic weather, the multitude of sources make the air quality problem in South Korea very complex.

Detailed measurements with back trajectories and statistical source-receptor models have been widely used to identify emission sectors and potential regions of sources (Kang et al., 2004; Park and Kim, 2005; Kim et al., 2007; Heo et al., 2009; Choi et al., 2013; Jeong et al., 2017). Modelers have traditionally used forward sensitivity analysis for source attribution (Jeon et al., 2014; Kim et al., 2017a, 2017b), which is straightforward to diagnose impacts of a change of specific emissions on $PM_{2.5}$ in South Korea. However, this approach is limited because of a small number of emission species/sectors/regions that can be evaluated in a computationally expedient manner.

Recently, adjoint sensitivity analysis has been used for source attribution of $PM_{2.5}$ in Seoul (the capital of South Korea) (Lee et al., 2017). Adjoint sensitivity analysis calculates sensitivities of $PM_{2.5}$ with respect to emissions from each species/sector/grid cell at once in a single backward integration. Lee et al. (2017) compared daily average simulated and observed $PM_{2.5}$ in Seoul for five years of May from 2009 to 2013. Then, they conducted adjoint sensitivity analysis targeting periods where both simulated and observed daily $PM_{2.5}$ were higher than 50 $\mu g\ m^{-3}$. They provided quantitative information of relative contributions of each species and regions. The results showed that for the high $PM_{2.5}$ events in Seoul, anthropogenic NH_3 emissions have the largest impacts. They also showed that the contribution of eastern China emissions is 69%, while the contribution of South Korea emissions is 15%.

KORUS-AQ, an intercontinental cooperative air quality field study in South Korea, was developed jointly by South Korea (national institutes and universities) and the United States (NASA, NCAR, and universities) in May–June, 2016. The KORUS-AQ aimed at improving our understanding of the factors contributing to poor air quality in South Korea. The study collected extensive observations of $PM_{2.5}$ and its related species from aircraft, ground sites, and ships. During the campaign, both local and transboundary pollution under different synoptic conditions were identified. The KORUS-AQ offers the best opportunity to investigate complex contributions of different sources to $PM_{2.5}$ in South Korea. This would enable us to determine which source would be an effective target in reducing the averaged population exposure to $PM_{2.5}$ in South Korea.

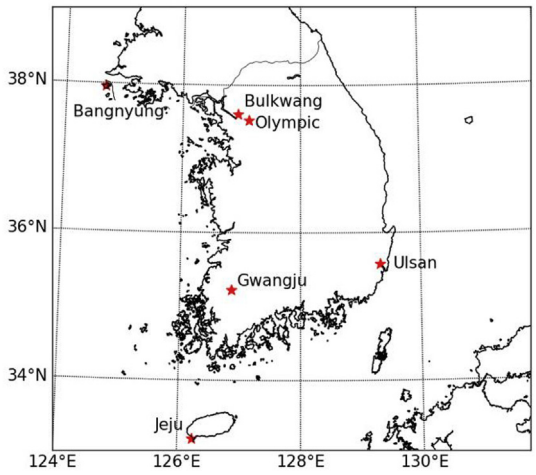

Fig. 1. Locations of six ground sites during the KORUS-AQ: Bangnyung (37.96° N, 124.67° E), Olympic park (37.52° N, 127.12° E), Bulkwang (37.61° N, 126.94° E), Gwangju (35.23° N, 126.85° E), Ulsan (35.58° N, 129.32° E), and Jeju (33.21° N, 126.23° E).

Many previous studies discussed above (e.g., Lee et al., 2017) investigated sources of $PM_{2.5}$ in specific regions in South Korea (e.g. Seoul) and during episodic events (e.g. transboundary pollution). However, it is not possible to apply those results to the whole country. Moreover, sources of a high $PM_{2.5}$ case under strong transport are expected to be very different from other cases because synoptic conditions determine sources and pollution events. To address these issues, we investigate sources of $PM_{2.5}$ in South Korea using extensive observations and modeling under various meteorological conditions during the KORUS-AQ campaign. In addition, we provide quantitative information of source contributions to $PM_{2.5}$ in South Korea for policymakers.

2. Observations during the KORUS-AQ

Supporting observations during the KORUS-AQ include hourly $PM_{2.5}$ and its constituents (SO_4^{2-}, NO_3^-, NH_4^+, OC, and EC) measured at six ground sites (Fig. 1) from May 10th to June 10th. We use observations at the Olympic Park ground site by Seoul Metropolitan Government Research Institute of Public Health and Environment during the KORUS-AQ. The other five ground sites have conducted year-round measurements, operated by South Korea's National Institute of Environmental Research (NIER). For $PM_{2.5}$ measurements, a radiometric particulate mass monitor, FH62C14 (Thermo Scientific, USA) was used at Olympic Park, and the beta-ray attenuation method, BAM-1020 (Met One Instruments, Inc., USA) was used at other sites.

At Olympic Park, the Monitor for Aerosols & Gasses in Ambient Air, MARGA ADI2080 (DOGA Limited, Turkey) measured SO_4^{2-}, NO_3^-, and NH_4^+. At other sites, the anion and cation particle and gas system, AIM URG-9000D (URG Corporation, USA) was used for SO_4^{2-}, NO_3^-, and NH_4^+ measurements. Both MARGA and AIM include ion chromatography for separating ions and polar molecules based on the charge properties of the molecules. For measuring OC and EC, the Model-4 Semi-continuous OC-EC Field Analyzer (SOCEC, Sunset Laboratory Inc., USA) was used at all sites.

KORUS-AQ experienced various meteorological conditions and we refer readers to NIER and NASA (2017) for its detailed description; here we provide a brief overview. The KORUS-AQ campaign occurred in May–June in South Korea with general climate conditions of warm temperature, high humidity, and long daylights that affect chemical reactions and natural emissions from vegetation. The campaign did not focus on strong transport and episodic events of soil dust and pollution periods, which are usually problematic in wintertime or springtime in

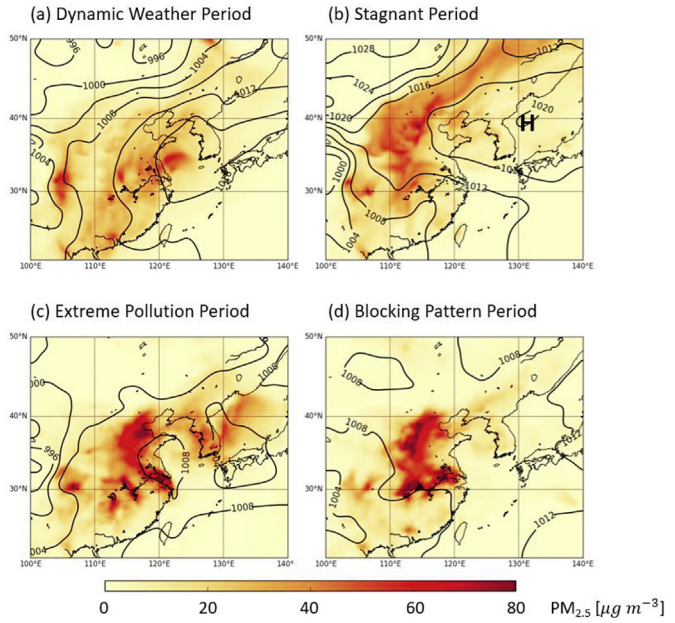

Fig. 2. Mean sea level pressures (contours, hPa) and mean concentrations of surface $PM_{2.5}$ (colors, $\mu g\ m^{-3}$) during each period under different meteorological conditions; (a) dynamic weather period, (b) stagnant period, (c) extreme pollution period, and (d) blocking pattern period. (For interpretation of the references to color in this figure legend, the reader is referred to the Web version of this article.)

South Korea. Hence, we could focus more on local sources examining what can be achieved only by domestic regulations.

Four different meteorological conditions were identified during the KORUS-AQ: dynamic weather period, stagnant period, extreme pollution period, and blocking period. Fig. 2 shows the mean sea level pressures and mean concentrations of $PM_{2.5}$ during each of the four periods. During the dynamic weather period (May 10-16), there was a rapid cycle of clear and rainy days. The stagnant period (May 17-22) was under the influence of a persistent high pressure system. The period showed building up of local pollution, indicating a substantial influence of local emissions. During the extreme pollution period (May 25-28), there was strong direct transport from China. The $PM_{2.5}$ air quality violations (more than 50 $\mu g\ m^{-3}$ for a 24-h average concentration in 2016) were only observed during the extreme pollution period. The blocking period (June 1-7) was under the influence of a blocking pattern over East Asia. A contrast in synoptic meteorology between four periods enables us to compare source contributions under different meteorological conditions.

3. GEOS-Chem forward model

We use a 3-D global chemical transport model (GEOS-Chem, http://www.geos-chem.org) to conduct a fully coupled oxidants-aerosols simulation for the campaign. The GEOS-Chem includes detailed tropospheric gas-phase chemistry of the O_3-NO_x-VOCs chemical mechanism (Bey et al., 2001; Hudman et al., 2007) with externally mixed aerosols including H_2SO_4–HNO_3–NH_3 and carbonaceous aerosols (Park et al., 2003, 2004, 2006). An aerosol thermodynamic equilibrium between gases and aerosols is calculated using ISORROPIA II (Fountoukis and Nenes, 2007; Pye et al., 2009; Capps et al., 2012). Physical losses of gases and aerosols by wet and dry deposition are computed using the schemes by Liu et al. (2001), and by Wesely (1989), respectively.

For simulating $PM_{2.5}$ concentrations and its components in South Korea, we use a high-resolution nested version of GEOS-Chem, which is driven by assimilated meteorology from the Goddard Earth Observing System (GEOS) of the NASA Global Modeling and Assimilation Office (GMAO). We use GEOS-FP meteorological data with 0.25° × 0.3125° horizontal resolutions and 47 reduced vertical layers up to 0.01 hPa for the domain over Northeast Asia (20° N– 50° N, 100° E– 145° E). We compute boundary conditions in two steps. First, a global simulation with 2° × 2.5° is conducted to provide boundary conditions for a nested simulation over the Asia domain (11° N– 55° N, 70° E– 150° E). Then, the results from the nested simulation are used as boundary conditions and initial conditions for the smaller nested Northeast Asia simulation (20° N– 50° N, 100° E– 145° E). The smaller domain reduces the computational costs of heavy adjoint simulations for source attribution (Lee et al., 2017).

Table 1
Anthropogenic NH_3, NO_x, SO_2, OC, and BC emissions in May–June in KORUS ver. 2.0 inventory[a,b].

Region	NH_3	NO_x	SO_2	OC	BC
S.Korea	61	162	55	3	3
N.Korea	19	30	13	1	4
Liaoning	95	202	121	7	15
Beijing	288	569	435	18	39
Shandong	642	791	670	25	71
Shanghai	617	955	795	31	73
Japan	44	251	88	3	2
Other	1329	1511	1243	67	190
Total	3095	4471	3420	153	395

[a] Units are Tg.
[b] See Fig. 8 (a) for the definitions of eight source regions.

For anthropogenic emissions including ship emissions in the nested simulations, we use the KORUS ver. 2.0 inventory, which was updated from KORUS ver. 1.0 for the KORUS-AQ campaign by Konkuk University. The KORUS ver. 2.0 inventory is based on the NIER/KU-CREATE inventory for the year 2015 and is updated with a GAINS scenario for East Asia, the ANL (Argonne National Laboratory) inventory for South and Southeast Asia, and the REAS inventory for Japan (Woo et al., 2012). We present in Table 1 total emissions of anthropogenic NH_3, NO_x, SO_2, OC, and BC from the KORUS ver. 2.0 inventory. Biomass burning emissions are taken from the monthly GFED3 inventory (Giglio et al., 2010), and biogenic emissions are from MEGAN (Guenther, 2006). Natural emissions of NO_x are from lightning (Murray et al., 2012) and soil (Yienger and Levy, 1995; Wang et al., 1998). Natural emissions of NH_3 are from the GEIA inventory (Bouwman et al., 1997).

Following Zhu et al. (2015) and Lee et al. (2017), we apply diurnal variations of NH_3 emissions. We use the scheme for livestock emissions as proxy for anthropogenic NH_3 emissions from all sectors. As Lee et al. (2017) suggested, diurnal profiles of NH_3 emissions for other sectors such as mobile sources should be developed to represent NH_3 in urban areas in South Korea.

Photolysis of particulate nitrate has recently been reported to be a major source of daytime HONO and NO_x (Ye et al., 2016), and could be an additional loss reaction of particulate nitrate during the daytime. Rate constants have been examined by laboratory experiments using aerosol samples collected from ground sites and aircrafts (Ye et al., 2017). Seungun Lee (personal communication) implemented particulate nitrate photolysis reactions in the GEOS-Chem to examine its impacts on simulated HONO and NOx during the KORUS-AQ campaign. The model also significantly reduced the high bias of nitrate concentrations, resulting in a better agreement with the observations during the campaign. We follow the scheme of Seungun Lee (personal communication) and add the photolysis of particulate nitrate (Eq. (1)) assuming a simple photolysis rate $j(NO_3^-)$ as a function of solar zenith angle (SZA) (Eq. (2)). However, reaction parameters including the yield constants and the photolysis rates are still uncertain yet, which require further investigation.

$$3NO_3^- \rightarrow NO_2 + 2HONO \quad (1)$$

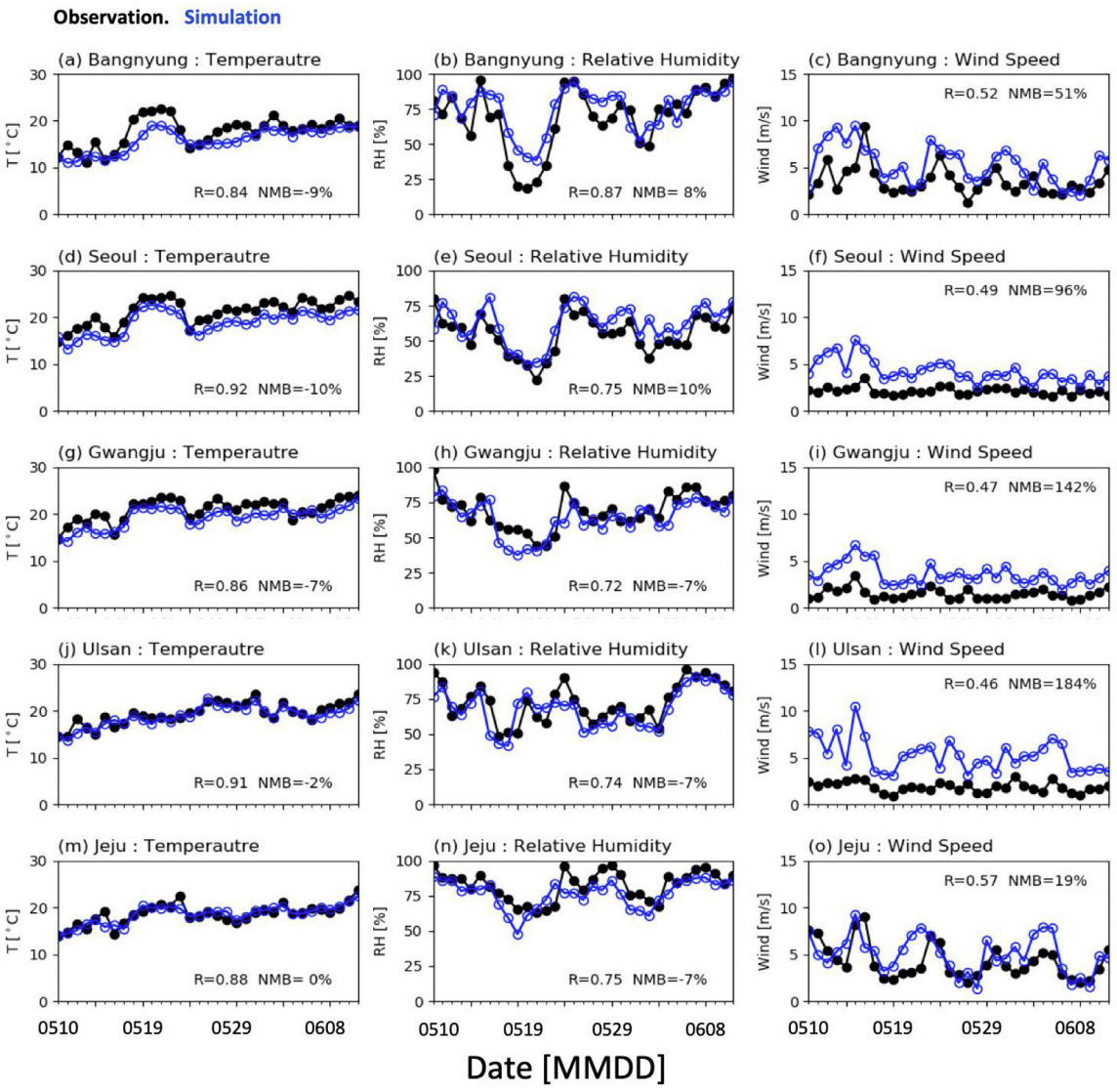

Fig. 3. Daily averaged temperature [°C], relative humidity [%] and wind speed [m/s] at five ground sites during the KORUS-AQ, in May–June 2016. Black filled circles are observations and blue open circles are GEOS-FP meteorological conditions. (For interpretation of the references to color in this figure legend, the reader is referred to the Web version of this article.)

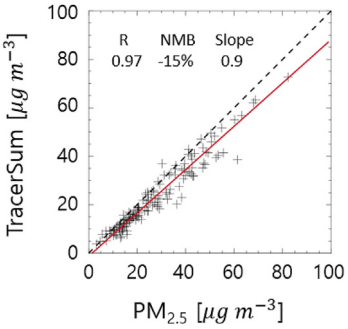

Fig. 4. Daily average $PM_{2.5}$ concentrations at six ground sites during the KORUS-AQ. X-axis is the $PM_{2.5}$ measured by FH61C14 and BAM-1020. Y-axis is the tracer sum of SO_4^{2-}, NO_3^-, NH_4^+, EC, and 2.1×OC measured by MARGA ADI2080, AIM URG-9000D, and SOCEC.

$$j(NO_3^-) = 2.0 \times 10^{-4} \times \cos(SZA) \quad (2)$$

Organic aerosol (OA) in GEOS-Chem has shown large discrepancies when compared to the observations because of the limited capability to simulate secondary organic aerosols (SOA) (Heald et al., 2005; Volkamer et al., 2006). The complex SOA formation of such simulations is primarily based on gas-particle partitioning of semi-volatile organics (Pankow, 1994b, a; Odum et al., 1996). Recently, many studies have shown that inclusion of chemical aging reactions in the atmosphere leads to decreases in organic volatility and increases in SOA mass yields, improving SOA simulation significantly (Donahue et al., 2006; Volkamer et al., 2006; Kroll and Seinfeld, 2008; Jimenez et al., 2009). Jo et al. (2013) implemented chemical aging reactions of SOA in the GEOS-Chem by using the volatility basis set (VBS) approach and showed that increases of SOA production and burden reduced the gap between the observations and the model.

The standard GEOS-Chem model used for source attribution (the forward model of the GEOS-Chem adjoint) does not include any SOA schemes. Lack of SOA formation leads to significant low bias of organic aerosol simulation. Therefore, we add a simple SOA formation from anthropogenic aromatic species (benzene, toluene, xylene) using Eqs. (3)–(6). The rationale for the implementation is that anthropogenic aromatics have the largest contribution to modeled SOA formation in East Asia. The SOA produced from anthropogenic aromatics accounts for 92.2% of total SOA in East Asia during the KORUS-AQ, which is

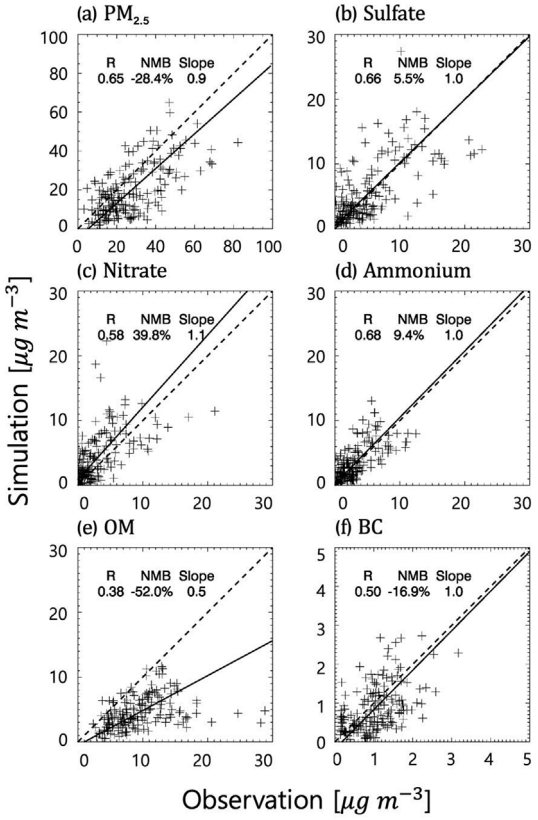

Fig. 5. Scatter plots of daily average (a) $PM_{2.5}$, (b) sulfate, (c) nitrate, (d) ammonium, (e) OM, and (f) BC at 6 ground sites during the KORUS-AQ between the observations (x-axis) and the simulation (y-axis).

calculated from our GEOS-Chem forward model simulation using the VBS approach with chemical aging (Jo et al., 2013).

$$AROM + OH \rightarrow ARO2 \quad (3)$$

$$ARO2 + NO \rightarrow LARO2N \quad (4)$$

$$ARO2 + HO_2 \rightarrow LARO2H \quad (5)$$

$$SOA = \alpha \times (LARO2N + LARO2H) \times \gamma \quad (6)$$

where AROM includes benzene, toluene, and xylene, ARO2 is the oxidation product of aromatics by OH, LARO2N and LARO2H are intermediate species to track oxidation of ARO2 by NO or by HO_2, α is gas phase SOA yield parameter, $\alpha \times (LARO2N + LARO2H)$ is secondary organic gas-phase semivolatile product (SOG), and γ is the ratio which represents aerosol fraction of aromatic SOA as described in detail below.

SOG formation from aromatic oxidations follows Henze et al. (2008) and α values are from Ng et al. (2007), assuming a high-NO_x condition in East Asia. However, instead of calculating reversible SOA formation, we irreversibly convert SOG to SOA by multiplying SOG by γ, which is computed in advance (Eq. (7)), by running a nested simulation of the GEOS-Chem using the VBS approach with chemical aging (Jo et al., 2013) for East-Asia during the KORUS-AQ campaign.

$$\gamma = SOA/(SOA + SOG) \quad (7)$$

where SOA is the average SOA budget and SOG is the average SOG budget of the GEOS-Chem nested simulation considering the VBS approach with aging. Calculated γ is 0.88 for East Asia during the KORUS-AQ campaign.

We define $PM_{2.5}$ as the sum of SO_4^{2-}, NO_3^-, NH_4^+, BC, 2.1×POC, and SOA from the model. The conversion factor 2.1 is used to convert primary OC (POC) to organic matter ($OM = 2.1 \times POC + SOA$) (Turpin and Lim, 2001; Philip et al., 2014). We estimate population exposure to $PM_{2.5}$ in South Korea, by calculating population-weighted average surface $PM_{2.5}$ at five ground sites during the KORUS-AQ (Olympic park, Bulkwang, Gwangju, Ulsan, and Jeju). We exclude $PM_{2.5}$ at the Bangnyung site in our analysis because of the very small population (~5000). The Olympic park and Bulkwang sites are located in Seoul but at the opposite side of the Han River. Therefore, we use the population of the southern part of Seoul (Gangnam, 5.3 million) for the Olympic park site and the northern part of Seoul (Gangbuk, 5.0 million) for the Bulkwang site. The populations of Gwangju, Ulsan, and Jeju are 1.5 million, 1.1 million, and 0.6 million, respectively.

4. GEOS-Chem adjoint model and adjoint sensitivity analysis

For source attribution, we use the GEOS-Chem adjoint v35 k (Henze et al., 2007). The adjoint model is an efficient tool for calculating gradients of a scalar model response with respect to numerous model parameters. The tool can be utilized for adjoint sensitivity analysis or inverse modeling depending on which scalar model response we focus on (tracer concentrations or model uncertainties). In this study, we investigate adjoint sensitivities of $PM_{2.5}$ with respect to emissions from each species/sector/grid cell. We define normalized sensitivity as

$$\lambda_{E,site,period} \equiv \frac{\partial J_{site,period}}{\partial E} \cdot \frac{E}{J_{site,period}} \times 100\ [\%] \quad (8)$$

where $\frac{\partial J_{site,period}}{\partial E}$ is found from solutions of the adjoint model. Here E is the emission of each $PM_{2.5}$ precursor in a single grid-cell, and. is the scalar model response called the cost function.

$$J_{site,period} = \frac{1}{M} \sum_{i=1}^{N} \sum_{j=1}^{M} c_{i,j} \quad (9)$$

where $c_{i,j}$ is the daily average surface concentration of aerosol species i comprising $PM_{2.5}$ in the grid-cell of the site on day j, M is the number of days during each period defined in Sect. 2, and N is the number of tracers comprising $PM_{2.5}$ (SO_4^{2-}, NO_3^-, NH_4^+, BC, OM). In this study, we define 20 cost functions, each of which is average surface $PM_{2.5}$ in the grid cell containing each of the five ground sites (Olympic park, Bulkwang, Gwangju, Ulsan, and Jeju) during each of the four periods (the dynamic weather period, the stagnant period, the extreme pollution period, and the blocking period) during the KORUS-AQ. We discuss in details the definition of the cost functions used in the study in Sect. 5.

After calculating the normalized sensitivities of 20 cost functions, we post-process the results to estimate total contributions from all emissions to population exposure to $PM_{2.5}$ in South Korea during each of the four periods (Fig. 7), which are calculated using Eq. 10 and 11.

$$\lambda_{period} = \frac{\sum_{site} (\sum_E \lambda_{E,site,period} \times Weight_{site,period})}{\sum_{site} (Weight_{site,period})} \quad (10)$$

$$Weight_{site,period} = J_{site,period} \times Population_{site} \quad (11)$$

where λ_{period} is total contributions from all emissions to population exposure to $PM_{2.5}$ in South Korea during a period, $\sum_E \lambda_{E,site,period}$ is total contributions from all emissions to $PM_{2.5}$ in a site during a period, $Weight_{site,period}$ is weighting factor, $Population_{site}$ is the population of the city for a site, and other notations are defined as the same ways as in Eqs. (8) and (9).

Next, we focus on emission source contributions to population exposure to $PM_{2.5}$ in South Korea during the KORUS-AQ (Fig. 8), which are defined as

$$\lambda_E = \frac{\sum_{site,period} (\lambda_{E,site,period} \times Weight_{site,period})}{\sum_{site,period} (Weight_{site,period})} \quad (12)$$

where λ_E is contribution of emission source E to population exposure to $PM_{2.5}$ in Korea during the KORUS-AQ, and other notations are defined

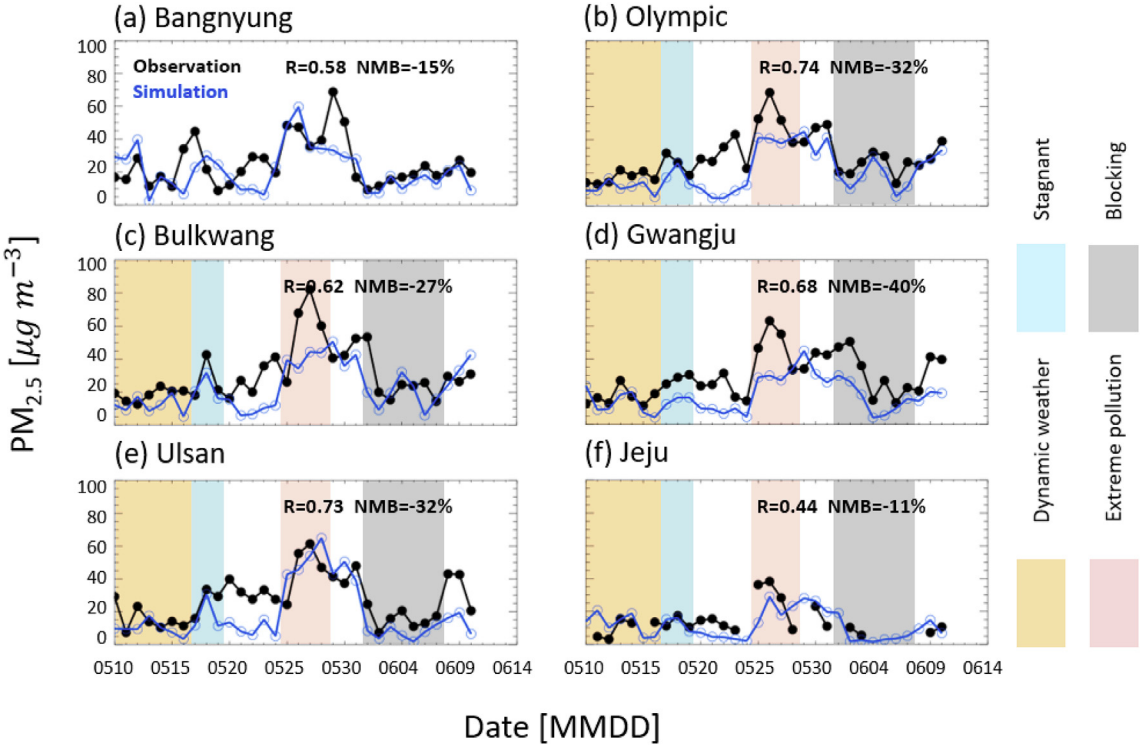

Fig. 6. Daily average $PM_{2.5}$ at six ground sites during the KORUS-AQ, in May–June 2016. Black filled circle is observed $PM_{2.5}$ and blue open circle is simulated $PM_{2.5}$. Shadings indicate four periods under different meteorological conditions: yellow– the dynamic weather period, light blue – the stagnant period (We exclude 20th-22nd May, when the model doesn't capture the increment in the observations), red – the extreme pollution period, and grey – the blocking period. We use daily average $PM_{2.5}$ in each shading as the cost function for source attribution. (For interpretation of the references to color in this figure legend, the reader is referred to the Web version of this article.)

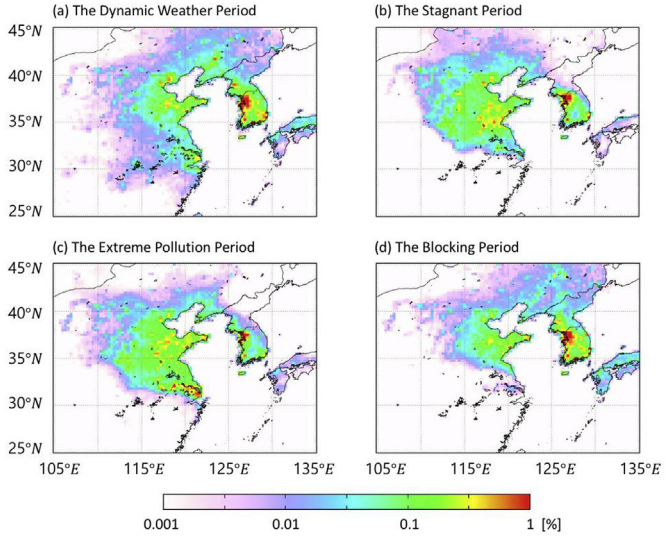

Fig. 7. Cost function-weighted and population-weighted total contributions from all emissions to $PM_{2.5}$ in South Korea under different meteorological conditions.

as the same ways as in Eq. 10 and 11.

5. Model evaluation

Prior to evaluating the simulated PM2.5 concentrations, we first conduct validations of meteorological data that drive model simulations. Fig. 3 shows comparisons for temperature, relative humidity, and wind speed between the GEOS-FP meteorological data and in-situ observations at five ground sites (Bangnyung, Seoul, Gwangju, Ulsan, and Jeju Gosan). The observations are obtained using Automated Synoptic Observing System (ASOS) by Korea Meteorological Administration (http://data.kma.go.kr). In general, temperature and relative humidity show good agreements with the observations. We find that the GEOS-FP wind speed data are higher than the observed surface wind, which typically occurs in weather forecasting results and even in the reanalysis data because of insufficient representation of surface conditions in the model. This may cause a low bias in simulated $PM_{2.5}$ especially for primary species.

We conduct the forward model evaluation by comparing the model with observations at six ground sites during the KORUS-AQ. The observations include daily mean concentrations of $PM_{2.5}$ and its chemical components.

Fig. 4 shows a comparison between $PM_{2.5}$ concentrations and the sum (TracerSum) of species comprising $PM_{2.5}$ measured at six ground sites during the KORUS-AQ. The concentrations of $PM_{2.5}$ were directly measured by FH62C14 and BAM-1020. The TracerSum is defined as the same way we define $PM_{2.5}$ in the model as the sum of SO_4^{2-}, NO_3^-, NH_4^+, BC, and OM (2.1×OC), which were measured by MARGA ADI2080, AIM URG-9000D, and SOCEC. A correlation coefficient between the TracerSum and the $PM_{2.5}$ measurements is 0.97. The TracerSum is 15% lower than the $PM_{2.5}$ measurements, which include contributions from crustal elements (Sajeev et al., 2017). Although the TracerSum is the best observations for evaluation, we instead use the $PM_{2.5}$ measurements for evaluating the model because there are less number of days with missing data in the direct $PM_{2.5}$ measurements (16) than in the TracerSum (48) out of 198 data points (33 *days* × 6 *sites*).

Fig. 5 shows comparisons of $PM_{2.5}$ and its species between the simulation and the observations. The model underestimates $PM_{2.5}$ by 29%. The low bias of $PM_{2.5}$ in the model is partly because the simulated $PM_{2.5}$ does not also include crustal elements and because the model

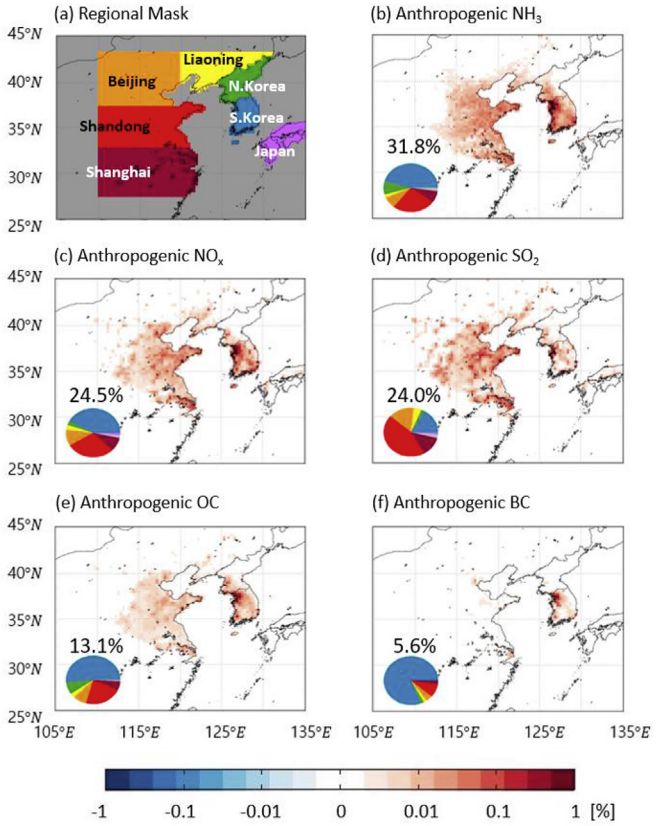

Fig. 8. (a) Eight source regions indicated by different colors: blue – South Korea, green – North Korea, yellow – Liaoning region, orange – Beijing region, red – Shandong region, dark red – Shanghai region, purple – Japan, grey – the rest of the domain. (b–f) spatial distributions of contributions from the five most important emission sources to population exposure to $PM_{2.5}$ in South Korea during the KORUS-AQ: (b) anthropogenic NH_3, (c) NO_x, (d) SO_2, (e) OC, and (f) BC. Pie charts indicate regional contributions. Total contributions from each emission species are written above pie charts. (For interpretation of the references to color in this figure legend, the reader is referred to the Web version of this article.)

Table 2
Regional contributions to population exposure to $PM_{2.5}$ in South Korea by period [%][a].

	Dynamic Weather	Stagnant	Extreme Pollution	Blocking
South Korea	50	34	26	57
North Korea	6	4	3	9
Liaoning Region	6	2	2	3
Beijing Region	9	16	10	6
Shandong Region	17	39	38	17
Shanghai Region	6	2	18	~0
Japan	2	~0	~0	2
Rest of the domain	4	2	2	6

[a] See Fig. 8 (a) for the definitions of eight source regions.

underestimates OM. The low bias of OM has decreased after implementing SOA formation from the aromatics in the model (NMB from −68% to −52%), but the discrepancy is still high. The use of an explicit SOA formation with a VBS scheme would further decrease this low bias in the model, which will be conducted in the future. Also, modeling detailed chemistry of biogenic and aromatic volatile organic compounds (VOCs) would improve SOA simulations (Fu et al., 2008; Zhang et al., 2014; Marais et al., 2016; Li et al., 2017; Porter et al., 2017).

Simulated nitrate is overestimated by 40%, whereas simulated sulfate, ammonium, and BC are generally in good agreements with the observations (NMBs are 6%, 10%, −17%, respectively). The high bias of nitrate has decreased after applying diurnal variations of NH_3 emissions (NMB from 268% to 155%) and after implementing the photolysis of particulate nitrate (NMB = 69%). Diurnal variations of NH_3 emissions also improve the simulated diurnal variations of nitrate (Fig. S1), by reducing night-time nitrate concentrations. However, two updates do not fully resolve the problem. Inclusion of the explicit SOA formation has improved the nitrate simulation further (NMB = 40%) because an additional aromatic oxidation by OH leads to decreases in OH concentrations, which decelerate HNO_3 production and thus nitrate formation.

Fig. 6 shows comparisons between the simulated and observed daily average $PM_{2.5}$ at 6 ground sites during the KORUS-AQ, in May–June 2016. Except for the period when the model does not capture the increment in the observations (May 20-24), the model generally reproduces the daily variations of the observations. The correlation coefficient ranges from 0.44 (Jeju) to 0.74 (Olympic park) and NMB is from −40% (Gwangju) to −11% (Jeju). Shadings indicate four periods under different meteorological conditions as described in Sect. 2: yellow - the dynamic weather period, light blue - the stagnant period (20^{th}-22nd May excluded), red - the extreme pollution period, and grey - the blocking period. As described in Sect. 4, we define 20 cost functions excluding Bangnyung for source attribution as daily average $PM_{2.5}$ at five ground sites during four periods as indicated with different color shading.

6. Source contributions to $PM_{2.5}$ in South Korea during the KORUS-AQ

For each cost function shown in Fig. 6, we conduct an adjoint sensitivity analysis for source attribution. We calculate contributions of each emission source by integrating normalized sensitivities (Eq. (8)) from the end of each episode to five days prior to the onset of the episode. This enables us to identify contributions of each emission source to $PM_{2.5}$ at each of the five sites during each of the four periods during the KORUS-AQ.

Next, we examine how regional contributions vary with meteorological conditions by using Eq. 10 and 11. Fig. 7 shows total contributions from all emissions to population exposure to $PM_{2.5}$ in South Korea during each of the four periods. Table 2 summarizes corresponding regional contributions. For comparing regional contributions, we define eight source regions in Fig. 8 (a): South Korea, North Korea, Liaoning region, Beijing region, Shandong region, Shanghai region, Japan, and the rest of the domain. During the extreme pollution period, the Chinese contribution (the sum of Liaoning region, Beijing region, Shandong region, and Shanghai region contributions) is 68%, whereas the domestic contribution is 26%. The high contribution from Chinese emissions during the extreme pollution period is consistent with the findings of Lee et al. (2017). However, we find that Chinese contributions vary widely depending on meteorological conditions. In particular, during the blocking period, the Chinese contribution is reduced to 25%.

Local emissions play a substantial role during the blocking period (57%) and during the dynamic weather period (50%). We also recognize that the model fails to capture the building up of local pollution at the end of the stagnant period on May 20–22. Because we exclude the period for the analysis, it is possible that the local contribution during the stagnant period (34%) is underestimated.

We estimate the five most important emission sources to population exposure to $PM_{2.5}$ in South Korea during all four periods of the KORUS-AQ as described in Eq. (12) (Fig. 8). Population exposure to $PM_{2.5}$ in South Korea is most sensitive to anthropogenic NH_3 emissions. Anthropogenic NO_x emissions have the second important role in reducing population exposure to $PM_{2.5}$, followed by anthropogenic emissions of SO_2, OC, and BC.

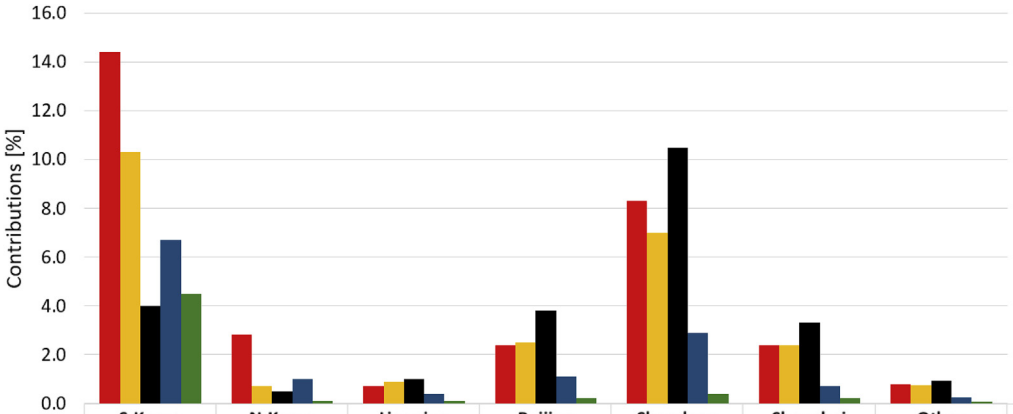

	S.Korea	N.Korea	Liaoning	Beijing	Shandong	Shanghai	Other	Sum
NH_3	14.4	2.8	0.7	2.4	8.3	2.4	0.8	31.8
NO_x	10.3	0.7	0.9	2.5	7.0	2.4	0.7	24.5
SO_2	4.0	0.5	1.0	3.8	10.5	3.3	0.9	24.0
OC	6.7	1.0	0.4	1.1	2.9	0.7	0.3	13.1
BC	4.5	0.1	0.1	0.2	0.4	0.2	0.1	5.6
Sum	39.9	5.1	3.1	10.0	29.1	9.0	2.7	98.9

Fig. 9. Effectiveness of incremental control of anthropogenic emission from each region/species on reducing population exposure to $PM_{2.5}$ in South Korea during the KORUS-AQ. See Fig. 8 (a) for the definitions of eight source regions.

Regional contributions, summarized in the pie charts in Fig. 8 indicate substantial local productions. Half of ammonium, nitrate, and organic aerosols are from local sources. The domestic contribution is dominant for BC. However, anthropogenic SO_2 emissions show large external contributions due to sulfate aerosols, whose concentrations show sharp enhancement during the extreme pollution period.

Finally, we sum up contributions (λ_E) from all grid boxes for each region in Fig. 8 (a). We provide effectiveness of incremental control of anthropogenic emissions from each species/region in reducing population exposure to $PM_{2.5}$ in South Korea (Fig. 9). We consider incremental changes because adjoint sensitivities are the local tangent gradient and may not reflect contributions at the zero-out level. Effectiveness in Fig. 9 indicates the largest response per change in emission. Except for anthropogenic SO_2 emissions, local controls have the best chance to improve $PM_{2.5}$ air quality in South Korea. Reduction of anthropogenic NH_3 emissions from South Korea is most effective in reducing the population exposure to $PM_{2.5}$ in South Korea. Anthropogenic SO_2 emissions from Shandong region are the second most effective target for reduction. Local regulation in anthropogenic NO_x emissions is effective as well. Reductions in anthropogenic NH_3 emissions from Shandong and anthropogenic NO_x emissions from Shandong also have a good chance to affect $PM_{2.5}$ air quality in South Korea. Although emissions from Shanghai are higher than Shandong except for NH_3 (Table 1), Shandong emissions show larger contributions to $PM_{2.5}$ in South Korea. This again indicates an important role of the meteorological conditions during the campaign.

We also provide the same information but during each of the four periods (Table S1). The order of the importance of emission species is similar for all the periods, showing the largest contribution from anthropogenic NH_3 emissions (28.2–34.1%). However, as shown in Fig. 7, regional contributions vary a lot, depending on the meteorological conditions.

Our adjoint sensitivity analysis strongly depends on the forward model simulation of $PM_{2.5}$. It should be noted that high bias in nitrates (40%) and low bias in OM (−52%) might have caused skewed adjoint sensitivities of $PM_{2.5}$ to certain emissions such as emissions of NO_x, NH_3, OC, or aromatic species. Spatial patterns are similar for $PM_{2.5}$ adjoint sensitivities to the emissions of NO_x, NH_3, and OC (Fig. 8) and the pie charts show strong local influences (Fig. 8). This indicates that about half of nitrate and primary OC aerosols are from South Korea. Therefore, regional contributions may not be significantly changed if the fraction of nitrate decreases and the fraction of primary OC increases. However, that is not the case if the fraction of SOA is the problem for the underestimation of OM or if specific sources and processes are excluded in the current forward model. Further investigations are needed to improve the forward model for better source attribution estimates.

7. Conclusion

Emission sources of $PM_{2.5}$ in South Korea during the KORUS-AQ campaign are investigated using the adjoint of GEOS-Chem. The model is updated with the up-to-date local emission inventory for the KORUS-AQ campaign, the KORUS ver. 2.0 inventory, with diurnal varying NH_3 emissions, photolysis of particulate nitrate, and SOA formation from aromatic species. The model is evaluated against observed $PM_{2.5}$ and its species at six ground sites located over South Korea. The updated model shows improved performance in simulating nitrate (NMB decreases from 268% to 40%) and organic aerosol (NMB increases from −68% to −52%). The simulated $PM_{2.5}$ underestimates the observations by 29% due to missing crustal materials in the simulation and due to the model underestimation of OM. Using the adjoint sensitivity analysis, source contributions to $PM_{2.5}$ at five ground sites during four periods of the KORUS-AQ are calculated. Four periods are characterized by different meteorological conditions, which are dynamic weather, stagnant, extreme pollution, and blocking pattern. Regional contributions are compared by periods. Chinese emissions show high contribution of 68% during the extreme pollution period. However, regional contributions show high variance with meteorological conditions. During the blocking period, Chinese contribution is only 25% and local contribution amounts to 57%. The effectiveness of incremental control of emission from individual species/regions on reducing population exposure to $PM_{2.5}$ in South Korea are provided. Reduction of anthropogenic NH_3 emissions from South Korea is most effective in reducing population exposure to $PM_{2.5}$ in South Korea. However, more importantly, we demonstrate that regional contributions depend largely on meteorological conditions and provide a means of quantifying the fluctuations in upwind contributions. As demonstrated by the title, this study aims at investigating source contributions during the KORUS-AQ. Because the campaign was selected for a time period with minimal

long-range transport influences, the quantitative regional contributions provided by this study can be considered as a lower bound on long-range transport influences. Therefore, further investigations for other years and other seasons are necessary for developing effective air quality mitigation strategies in South Korea. Especially, further studies are required for wintertime and summertime Korea when high and low $PM_{2.5}$ concentrations are characteristics. Also, it is necessary to study long term trends of source contributions.

Acknowledgments

We thank all members of the KORUS-AQ team for their contributions during the field campaign and the agencies operating the surface networks. This work was supported by the National Research Foundation of Korea (NRF) grant funded by the Korean government (MSIT) (No. 2018004494). Daven Henze was supported by "National Strategic Project-Fine particle of the National Research Foundation of Korea (NRF)" of the Ministry of Science and ICT (MSIT), the Ministry of Environment (ME), and the Ministry of Health and Welfare (MOHW). (2017M3D8A1092052).

Appendix A. Supplementary data

Supplementary data to this article can be found online at https://doi.org/10.1016/j.atmosenv.2019.02.008.

References

Beelen, R., Hoek, G., van Den Brandt, P.A., Goldbohm, R.A., Fischer, P., Schouten, L.J., Jerrett, M., Hughes, E., Armstrong, B., Brunekreef, B., 2008. Long-term effects of traffic-related air pollution on mortality in a Dutch cohort (NLCS-AIR study). Environ. Health Perspect. 116, 196.

Bey, I., Jacob, D.J., Yantosca, R.M., Logan, J.A., Field, B.D., Fiore, A.M., Li, Q., Liu, H.Y., Mickley, L.J., Schultz, M.G., 2001. Global modeling of tropospheric chemistry with assimilated meteorology: model description and evaluation. J. Geophys. Res.: Atmosphere 106, 23073–23095.

Bouwman, A., Lee, D., Asman, W., Dentener, F., Van Der Hoek, K., Olivier, J., 1997. A global high-resolution emission inventory for ammonia. Glob. Biogeochem. Cycles 11, 561–587.

Capps, S., Henze, D., Hakami, A., Russell, A., Nenes, A., 2012. ANISORROPIA: the adjoint of the aerosol thermodynamic model ISORROPIA. Atmos. Chem. Phys. 12, 527–543.

Choi, J.-K., Heo, J.-B., Ban, S.-J., Yi, S.-M., Zoh, K.-D., 2013. Source apportionment of $PM_{2.5}$ at the coastal area in Korea. Sci. Total Environ. 447, 370–380.

Donahue, N., Robinson, A., Stanier, C., Pandis, S., 2006. Coupled partitioning, dilution, and chemical aging of semivolatile organics. Environ. Sci. Technol. 40, 2635–2643.

Fountoukis, C., Nenes, A., 2007. ISORROPIA II: a computationally efficient thermodynamic equilibrium model for K+–Ca 2+–Mg 2+–NH 4+–Na+–SO 4 2−–NO 3−–Cl−–H 2 O aerosols. Atmos. Chem. Phys. 7, 4639–4659.

Fu, T.-M., Jacob, D.J., Wittrock, F., Burrows, J.P., Vrekoussis, M., Henze, D.K., 2008. Global budgets of atmospheric glyoxal and methylglyoxal, and implications for formation of secondary organic aerosols. J. Geophys. Res.: Atmosphere 113. https://doi.org/10.1029/2007JD009505.

Giglio, L., Randerson, J., Van der Werf, G., Kasibhatla, P., Collatz, G., Morton, D., DeFries, R., 2010. Assessing variability and long-term trends in burned area by merging multiple satellite fire products. Biogeosciences 7.

Guenther, C., 2006. Estimates of global terrestrial isoprene emissions using MEGAN (model of emissions of gases and aerosols from nature). Atmos. Chem. Phys. 6.

Heald, C.L., Jacob, D.J., Park, R.J., Russell, L.M., Huebert, B.J., Seinfeld, J.H., Liao, H., Weber, R.J., 2005. A large organic aerosol source in the free troposphere missing from current models. Geophys. Res. Lett. 32.

Henze, D.K., Hakami, A., Seinfeld, J.H., 2007. Development of the adjoint of GEOS-Chem. Atmos. Chem. Phys. 7, 2413–2433.

Henze, D.K., Seinfeld, J., Ng, N., Kroll, J., Fu, T.-M., Jacob, D.J., Heald, C., 2008. Global modeling of secondary organic aerosol formation from aromatic hydrocarbons: high-vs. low-yield pathways. Atmos. Chem. Phys. 8, 2405–2420.

Heo, J.B., Hopke, P.K., Yi, S.M., 2009. Source apportionment of $PM_{2.5<}$ in Seoul, Korea. Atmos. Chem. Phys. 9, 4957–4971. https://doi.org/10.5194/acp-9-4957-2009.

Hodzic, A., Madronich, S., Bohn, B., Massie, S., Menut, L., Wiedinmyer, C., 2007. Wildfire particulate matter in Europe during summer 2003: meso-scale modeling of smoke emissions, transport and radiative effects. Atmos. Chem. Phys. 7, 4043–4064.

Hudman, R.C., Jacob, D.J., Turquety, S., Leibensperger, E.M., Murray, L.T., Wu, S., Gilliland, A., Avery, M., Bertram, T.H., Brune, W., 2007. Surface and lightning sources of nitrogen oxides over the United States: magnitudes, chemical evolution, and outflow. J. Geophys. Res.: Atmosphere 112.

Jeon, W.-B.L., Hwa, W., Lee, S.-H., Park, J.-H., Kim, H.-G., 2014. Numerical study on the characteristics of high PM2.5 episodes in anmyeondo area in 2009. Journal of Environmental Science International 23, 249–259. https://doi.org/10.5322/JESI.2014.23.2.249.

Jeong, J.-H., Shon, Z.-H., Kang, M., Song, S.-K., Kim, Y.-K., Park, J., Kim, H., 2017. Comparison of source apportionment of PM 2.5 using receptor models in the main hub port city of East Asia: Busan. Atmos. Environ. 148, 115–127.

Jimenez, J., Canagaratna, M., Donahue, N., Prevot, A., Zhang, Q., Kroll, J.H., DeCarlo, P.F., Allan, J.D., Coe, H., Ng, N., 2009. Evolution of organic aerosols in the atmosphere. Science 326, 1525–1529.

Jo, D., Park, R., Kim, M., Spracklen, D., 2013. Effects of chemical aging on global secondary organic aerosol using the volatility basis set approach. Atmos. Environ. 81, 230–244.

Kang, C.-M., Lee, H.S., Kang, B.-W., Lee, S.-K., Sunwoo, Y., 2004. Chemical characteristics of acidic gas pollutants and PM2.5 species during hazy episodes in Seoul, South Korea. Atmos. Environ. 38, 4749–4760. https://doi.org/10.1016/j.atmosenv.2004.05.007.

Kim, B.-U., Bae, C., Kim, H.C., Kim, E., Kim, S., 2017a. Spatially and Chemically Resolved Source Apportionment Analysis: Case Study of High Particulate Matter Event. Atmospheric Environment.

Kim, E., Bae, C., Kim, H.C., Cho, J.H., Kim, B.U., Kim, S., 2017b. Regional contributions to particulate matter concentration in the Seoul metropolitan area, Korea: seasonal variation and sensitivity to meteorology and emissions inventory. Atmos. Chem. Phys. Discuss. 1–33. https://doi.org/10.5194/acp-2016-1114. 2017.

Kim, H.-S., Huh, J.-B., Hopke, P.K., Holsen, T.M., Yi, S.-M., 2007. Characteristics of the major chemical constituents of PM2.5 and smog events in Seoul, Korea in 2003 and 2004. Atmos. Environ. 41, 6762–6770. https://doi.org/10.1016/j.atmosenv.2007.04.060.

Kroll, J.H., Seinfeld, J.H., 2008. Chemistry of secondary organic aerosol: formation and evolution of low-volatility organics in the atmosphere. Atmos. Environ. 42, 3593–3624.

Laden, F., Schwartz, J., Speizer, F.E., Dockery, D.W., 2006. Reduction in fine particulate air pollution and mortality: extended follow-up of the Harvard Six Cities study. Am. J. Respir. Crit. Care Med. 173, 667–672.

Lee, H.-M., Park, R.J., Henze, D.K., Lee, S., Shim, C., Shin, H.-J., Moon, K.-J., Woo, J.-H., 2017. Source attribution for Seoul in May from 2009 to 2013 using GEOS-Chem and its adjoint model. Environ. Pollut. 221, 377–384. https://doi.org/10.1016/j.envpol.2016.11.088.

Li, J., Zhang, M., Wu, F., Sun, Y., Tang, G., 2017. Assessment of the impacts of aromatic VOC emissions and yields of SOA on SOA concentrations with the air quality model RAMS-CMAQ. Atmos. Environ. 158, 105–115.

Liu, H., Jacob, D.J., Bey, I., Yantosca, R.M., 2001. Constraints from 210Pb and 7Be on wet deposition and transport in a global three-dimensional chemical tracer model driven by assimilated meteorological fields. J. Geophys. Res.: Atmosphere 106, 12109–12128.

Marais, E.A., Jacob, D.J., Jimenez, J.L., Campuzano-Jost, P., Day, D.A., Hu, W., Krechmer, J., Zhu, L., Kim, P.S., Miller, C.C., 2016. Aqueous-phase mechanism for secondary organic aerosol formation from isoprene: application to the southeast United States and co-benefit of SO 2 emission controls. Atmos. Chem. Phys. 16, 1603–1618.

Miller, K.A., Siscovick, D.S., Sheppard, L., Shepherd, K., Sullivan, J.H., Anderson, G.L., Kaufman, J.D., 2007. Long-term exposure to air pollution and incidence of cardiovascular events in women. N. Engl. J. Med. 356, 447–458.

Murray, L.T., Jacob, D.J., Logan, J.A., Hudman, R.C., Koshak, W.J., 2012. Optimized regional and interannual variability of lightning in a global chemical transport model constrained by LIS/OTD satellite data. J. Geophys. Res.: Atmosphere 117.

Ng, N., Kroll, J., Chan, A., Chhabra, P., Flagan, R., Seinfeld, J., 2007. Secondary organic aerosol formation from m-xylene, toluene, and benzene. Atmos. Chem. Phys. 7, 3909–3922.

NIER and NASA, 2017. KORUS-AQ Rapid Science Synthesis Report.

OECD, 2018. Air Quality and Health: Exposure to PM2.5 Fine Particles – Countries and Regions (Database). http://doi.org/10.1787/96171c76-en, Accessed date: 6 August 2018.

Odum, J.R., Hoffmann, T., Bowman, F., Collins, D., Flagan, R.C., Seinfeld, J.H., 1996. Gas/particle partitioning and secondary organic aerosol yields. Environ. Sci. Technol. 30, 2580–2585.

Pankow, J.F., 1994a. An absorption model of gas/particle partitioning of organic compounds in the atmosphere. Atmos. Environ. 28, 185–188.

Pankow, J.F., 1994b. An absorption model of the gas/aerosol partitioning involved in the formation of secondary organic aerosol. Atmos. Environ. 28, 189–193.

Park, R.J., Jacob, D.J., Chin, M., Martin, R.V., 2003. Sources of carbonaceous aerosols over the United States and implications for natural visibility. J. Geophys. Res.: Atmosphere 108.

Park, R.J., Jacob, D.J., Field, B.D., Yantosca, R.M., Chin, M., 2004. Natural and transboundary pollution influences on sulfate-nitrate-ammonium aerosols in the United States: implications for policy. J. Geophys. Res.: Atmosphere 109.

Park, R.J., Jacob, D.J., Kumar, N., Yantosca, R.M., 2006. Regional visibility statistics in the United States: natural and transboundary pollution influences, and implications for the Regional Haze Rule. Atmos. Environ. 40, 5405–5423.

Park, S.S., Kim, Y.J., 2005. Source contributions to fine particulate matter in an urban atmosphere. Chemosphere 59, 217–226. https://doi.org/10.1016/j.chemosphere.2004.11.001.

Philip, S., Martin, R.V., Pierce, J.R., Jimenez, J.L., Zhang, Q., Canagaratna, M.R., Spracklen, D.V., Nowlan, C.R., Lamsal, L.N., Cooper, M.J., Krotkov, N.A., 2014. Spatially and seasonally resolved estimate of the ratio of organic mass to organic carbon. Atmos. Environ. 87, 34–40. https://doi.org/10.1016/j.atmosenv.2013.11.065.

Pope III, C.A., Burnett, R.T., Thun, M.J., Calle, E.E., Krewski, D., Ito, K., Thurston, G.D., 2002. Lung cancer, cardiopulmonary mortality, and long-term exposure to fine

particulate air pollution. Jama 287, 1132–1141.
Porter, W.C., Safieddine, S.A., Heald, C.L., 2017. Impact of aromatics and monoterpenes on simulated tropospheric ozone and total OH reactivity. Atmos. Environ. 169, 250–257.
Pye, H., Liao, H., Wu, S., Mickley, L.J., Jacob, D.J., Henze, D.K., Seinfeld, J., 2009. Effect of changes in climate and emissions on future sulfate-nitrate-ammonium aerosol levels in the United States. J. Geophys. Res.: Atmosphere 114.
Sajeev, P., Randall, V.M., Graydon, S., Crystal, L.W., Aaron van, D., Michael, B., Daven, K.H., Zbigniew, K., Chandra, V., Sarath, K.G., Qiang, Z., 2017. Anthropogenic fugitive, combustion and industrial dust is a significant, underrepresented fine particulate matter source in global atmospheric models. Environ. Res. Lett. 12, 044018.
Turpin, B.J., Lim, H.-J., 2001. Species contributions to PM2. 5 mass concentrations: revisiting common assumptions for estimating organic mass. Aerosol Sci. Technol. 35, 602–610.
Volkamer, R., Jimenez, J.L., San Martini, F., Dzepina, K., Zhang, Q., Salcedo, D., Molina, L.T., Worsnop, D.R., Molina, M.J., 2006. Secondary organic aerosol formation from anthropogenic air pollution: rapid and higher than expected. Geophys. Res. Lett. 33.
Wang, Y., Jacob, D.J., Logan, J.A., 1998. Global simulation of tropospheric O3-NO x-hydrocarbon chemistry: 1. Model formulation. J. Geophys. Res.: Atmosphere 103, 10713–10725.
Weber, R.J., Sullivan, A.P., Peltier, R.E., Russell, A., Yan, B., Zheng, M., De Gouw, J., Warneke, C., Brock, C., Holloway, J.S., 2007. A study of secondary organic aerosol formation in the anthropogenic-influenced southeastern United States. J. Geophys. Res.: Atmosphere 112.
Wesely, M., 1989. Parameterization of surface resistances to gaseous dry deposition in regional-scale numerical models. Atmos. Environ. 23, 1293–1304 1967.
WHO Regional Office for Europe, 2013. Health Effects of Particulate Matter: Policy Implications for Countries in Eastern Europe, Caucasus and Central Asia. World Health Organization Regional Office for Europe.
WHO, 2016. Ambient Air Pollution: a Global Assessment of Exposure and Burden of Disease. World Health Organization. http://www.who.int/iris/handle/10665/250141.
Woo, J.-H., Choi, K.-C., Kim, H.K., Baek, B.H., Jang, M., Eum, J.-H., Song, C.H., Ma, Y.-I., Sunwoo, Y., Chang, L.-S., 2012. Development of an anthropogenic emissions processing system for Asia using SMOKE. Atmos. Environ. 58, 5–13.
Ye, C., Zhou, X., Pu, D., Stutz, J., Festa, J., Spolaor, M., Tsai, C., Cantrell, C., Mauldin, R.L., Campos, T., 2016. Rapid cycling of reactive nitrogen in the marine boundary layer. Nature 532, 489–491.
Ye, C., Zhang, N., Gao, H., Zhou, X., 2017. Photolysis of Particulate Nitrate as a Source of HONO and NOx. Environmental Science & Technology.
Yienger, J., Levy, H., 1995. Empirical model of global soil-biogenic NOχ emissions. J. Geophys. Res.: Atmosphere 100, 11447–11464.
Zhang, X., Cappa, C.D., Jathar, S.H., McVay, R.C., Ensberg, J.J., Kleeman, M.J., Seinfeld, J.H., 2014. Influence of Vapor Wall Loss in Laboratory Chambers on Yields of Secondary Organic Aerosol, Proceedings of the National Academy of Sciences, 201404727.
Zhu, L., Henze, D., Bash, J., Jeong, G., Cady-Pereira, K., Shephard, M., Luo, M., Paulot, F., Capps, S., 2015. Global evaluation of ammonia bidirectional exchange and livestock diurnal variation schemes. Atmos. Chem. Phys. 15.